Low-Complexity Angle Estimation for Integrated Sensing and Communication

Pedro Victor Martins Castro, Francisco Rodrigo Porto Cavalcanti, Walter da Cruz Freitas Júnior and Gábor Fodor

***Abstract*— This paper has two objectives. The first objective is to propose the creation of a codebook for low-complexity angular estimation of targets in a monostatic radar configuration employing a fifth generation (5G) physical layer based on multiple input multiple output orthogonal frequency division multiplexing. The second objective is to characterize the performance of the proposed angle estimation algorithm so as to verify its suitability for integrated sensing and communication under a resource allocation policy, based on the number of allocated subcarriers to the sensing task and a desired estimation accuracy. Comparisons with the classical multiple signal classification algorithm via simulations show that the proposed estimation algorithm achieves good overall accuracy with reduced computational complexity.**

***Keywords*— integrated sensing and communication (ISAC), multiple input multiple output (MIMO), multiple signal classification (MUSIC), orthogonal frequency division multiplexing (OFDM).**

I. Introduction

The advent of fifth generation (5G) networks marked a pivotal shift in the telecommunications landscape, aiming to significantly enhance the capacity of cellular systems and lay the groundwork for the internet of things (IoT) revolution. While these networks have indeed bolstered IoT capabilities and become instrumental to the industry, they fall short in certain critical areas. For example, their ability to achieve an outdoor high precision positioning key performance indicator (KPI) is limited to roughly 10 m, as highlighted in recent studies [1].

In response to these limitations, the telecommunications industry is setting its sights on the sixth generation (6G) networks, which are envisioned to satisfy more strict KPIs [2]. Among the myriad of services anticipated to be enabled by 6G, integrated sensing and communication (ISAC) emerges as a strong candidate. ISAC's potential applications span across various domains, including smart transportation, smart cities and homes, sensing-assisted communications and environmental sensing. In the realm of industrial IoT, ISAC is poised to revolutionize object detection, localization and tracking using radio waves emitted by communication equipment [3].

The objective of ISAC is to achieve mutual performance gains by harmonizing communication and sensing functionalities. To achieve this, two key sensing functions have been introduced: detection, to ascertain the presence of a target, and estimation, to determine parameters such as the target's distance and angular position relative to an access point (AP).

The state-of-the-art in signal processing for ISAC, as detailed in recent literature [4], delves into the geometric spatial channel model and fundamental communication signals like orthogonal frequency division multiplexing (OFDM). It also evaluates the merits and drawbacks of various sensing parameter estimation techniques, including subspace methods like multiple signal classification (MUSIC) and estimation of signal parameters via rotational invariant techniques (ESPRIT), compressive sensing methods, and tensor-based approaches [4]. Despite the optimal estimates produced by these methods, they often come with high computational costs, exemplified by the eigen-decomposition (ED) in MUSIC [5] and the diminishing performance of compressive sensing methods as the number of estimated parameters increases [4].

Radio resource sharing among sensing and communications functionalities that use separate antenna arrays for each service has been proposed [6], [7]. The idea in those works is to enable separate simultaneous beams for each functionality. The work in [6] also employs a codebook, but it is designed to single-carrier systems. The work in [7], on the other hand, operates in a multi-carrier setting but, as mentioned above, it separates the two services in the spatial domain by employing a relatively complex least-squares solution to calculate the two sets of beamforming weights.

Different from the works in [6] and [7], we address a monostatic radar sensing scenario proposing to use a single antenna array for both sensing and communication while benefiting from the time and frequency capabilities of OFDM. We present a low-complexity solution for identifying multiple targets' angular positions, assuming sensing and communication share frequency-time resources under a Quality-of-Service (QoS) and accuracy allocation policy. For this purpose, we propose a codebook for angular estimation of network-disconnected targets. The codebook is designed to cover the area where the targets are expected to be located.

The rest of this work is organized as follows. First, we present the system model in Section II. Then, we propose a low-complexity solution in Section III. Next, we evaluate the performance of the proposed solution and we compare it with MUSIC, a classical angle spectrum estimation algorithm, in section IV. Finally, we present conclusions in Section V.

II. System Model

A. Scenario

The scenario is set in the R^2 plane which contains an AP equipped with a uniform linear array (ULA) with M antenna elements centered at the origin of the plane. In a rectangular

Pedro V. M. Castro, F. Rodrigo P. Cavalcanti and Walter da Cruz F. Jr. are affiliated with the Wireless Telecommunications Research Group (GTEL), Federal University of Ceará, Fortaleza-CE, Brazil, e-mails: {pedrovictor, rodrigo, walter}@gtel.ufc.br. G. Fodor is with Ericsson Research, Stockholm 164 80, Sweden, e-mail: gabor.fodor@ericsson.com. This work has been supported by CAPES and by ERICSSON Telecomunicações S/A via cooperation contract UFC-50.

region in the first and second quadrants, in the far-field of the ULA, there are K targets. Let d be the spacing between the M antenna elements, then the length of the ULA is $L = (M-1)d$. Thus, the radius of size $2L^2/\lambda$ of the circumference centered at the origin defines the boundary of the far-field and near-field of the ULA [8]. We define $\lambda = c/f_c$ as the wavelength of the carrier, in which f_c is the central carrier frequency and c is the speed of light. Fig. 1 illustrates the described scenario.

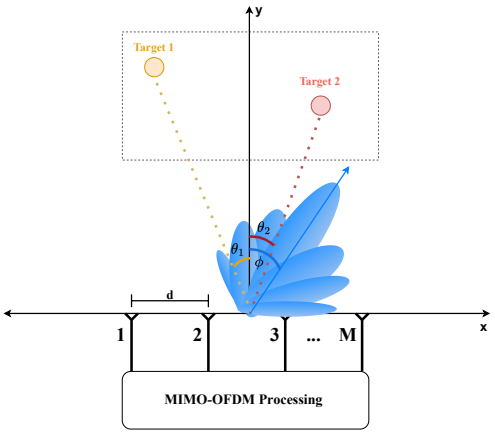

Fig. 1: Scenario.

Note that in Fig. 1, the radiation pattern has an angular direction ϕ, and targets 1 and 2 have angular positions θ_1 and θ_2, respectively. Notice that although the radiation pattern is directed towards a different direction from the targets' directions, electromagnetic waves still reach the targets with low gain in a line-of-sight (LoS) scenario. By means of appropriate adaptive beamforming techniques, the ULA is able to electronically scan the angular region of interest in search of targets. This search is carried out by sending multiple OFDM symbols in Q subcarriers, where $q \in \{0, 1, \cdots, Q-1\}$ is one particular subcarrier (SC), Δf is the spacing between SCs, and $B = Q \times \Delta f$ is the considered bandwidth. Thus, the considered system is a multiple input multiple output (MIMO)-OFDM system, as we are considering a case of monostatic ISAC using OFDM symbols in which the ULA acts as a multiple antenna array for both sensing signal transmitter and target echo receiver.

B. Channel

We define σ_k as the radar cross section (RCS) of target k. The Saleh-Valenzuela channel [9] dependent on the qth SC is defined as

$$\mathbf{H}_q(n) = \sum_{k=1}^{K} \beta_{q,k} e^{-j2\pi f_q \tau_k} e^{j2\pi f_{D_{q,k}} n T_s} \mathbf{a}(\theta_k)\mathbf{a}^T(\theta_k), \quad (1)$$

where $(.)^T$ represents the transpose operation, $n = \{1, 2, \cdots, N\}$ is the time-slot index among N time-slots available for sensing, $f_q = [q - (Q-1)/2]\,\Delta f + f_c$ is the frequency of the qth SC after modulation on f_c, $\tau_k = 2R_k/c$ is the round-trip delay for target k, where R_k is the distance between the center of the ULA and target k, $f_{D_{q,k}} = 2v_k/\lambda_q$ is the Doppler shift of target k for the qth SC, v_k is the radial velocity of target k and λ_q is the wavelength dependent on f_q.

We consider T_s as the symbol period and $\mathbf{a}(\theta_k) \in \mathcal{C}^{M\times 1}$ as the steering vector considering the angle θ_k of target k. The latter is defined as

$$\mathbf{a}(\theta_k) = \Big[e^{j\frac{2\pi}{\lambda_q}d\left(-\frac{M-1}{2}\right)sin(\theta_k)}, e^{j\frac{2\pi}{\lambda_q}d\left(1-\frac{M-1}{2}\right)sin(\theta_k)}, \cdots, e^{j\frac{2\pi}{\lambda_q}d\left(\frac{M-1}{2}\right)sin(\theta_k)}\Big]^T. \quad (2)$$

The term $\beta_{q,k}$ corresponds to the path-gain due to distance and the spreading of electromagnetic waves over the target. Thus, we model this term as the gain of the monostatic radar [10, Chapter 2]

$$\beta_{q,k} = \sqrt{\frac{\lambda_q^2 \sigma_k}{(4\pi)^3 R_k^4}}. \quad (3)$$

C. Signal Model

Let $\mathbf{B}_q \in \mathcal{C}^{M\times N}$ be a transmission matrix of the qth SC with a specific baseband digital modulation scheme for a ULA. The OFDM signal matrix without the addition of the cyclic prefix is defined as

$$\boldsymbol{\mathcal{B}}(t) = \frac{1}{\sqrt{Q}} \sum_{q=1}^{Q} \mathbf{B}_q e^{j2\pi f_q t}. \quad (4)$$

As we employ OFDM, we now incorporate the cyclic prefix into $\boldsymbol{\mathcal{B}}(t)$ to generate the final signal transmission matrix $\mathbf{C}(t)$ [11]. The echo received by the ULA on the qth SC is modeled according to (5).

$$\mathbf{X}_q(t) = \mathbf{H}_q \mathbf{C}(t) + \mathbf{Z}_q, \quad (5)$$

where each column of $\mathbf{Z}_q \in \mathcal{C}^{M\times N}$ follows a circularly symmetric complex Gaussian distribution with zero mean and covariance matrix equals $\alpha^2\mathbf{I} \in \mathcal{C}^{M\times M}$ and α^2 is the noise power dependent on Δf. Without loss of generality, we assume there is no intercarrier interference because, even when the targets do not move significantly during the round-trip delay for echo reception, it can be observed that the use of multiple antennas and beamforming techniques results in a reduction in the Doppler spread in MIMO-OFDM systems, which is indicative of a reduction in intercarrier interference [12]. Although the targets have some mobility, their angular positions are fixed when the signals are transmitted from the ULA.

D. Frame Structure

The utilized frame structure is similar to the structure presented by the 5G New Radio (5G NR) protocol [13]. That is, part of the initial access (IA) slots of the Synchronization Signal Block (SSB) is used to perform sensing over a specific angular region. The subcarrier spacing (SCS) to be considered in this work are also as the ones defined by the 5G NR standard [13]. So, one way to estimate the angular positions of the targets is to use at most 64 SSBs where each one occupies 4 symbols and 240 SCs [13]. The work in [14] presents the ISAC in a 5G NR protocol and elucidates the utilization of the SSBs in the IA frame in both conventional and ISAC schemes.

Although the focus is on estimating the angular positions of targets, this approach may encounter challenges due to temporal overlap among transmitted signals and received

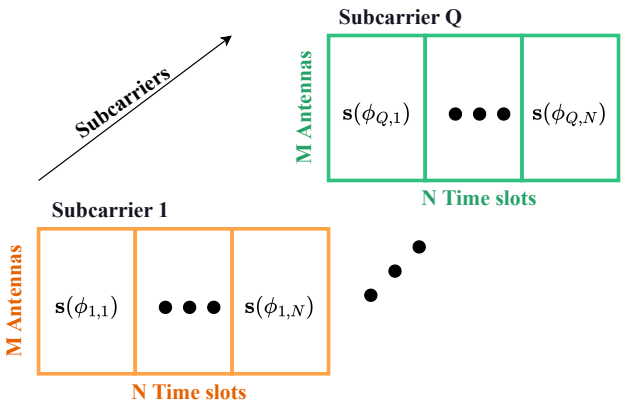

Fig. 2: OFDM matrices.

echoes. One solution to this problem is to adjust the SCS in order to reduce the duration of time-slots, thus allowing the echoes to arrive at a more favourable time instant. It is also possible to employ full-duplex techniques, such as Antenna Cancellation and Antenna Separation and Digital Cancellation (ASDC) [15].

III. Proposed Angle Estimation Solution

The proposed solution is based on the idea of creating $M \times N$ OFDM symbols such that these symbols cover the entire angular space where the K targets are present. It is important to notice that these designed symbols are pilots signals which form a codebook. To do this, we need to redesign the OFDM signal matrix $\boldsymbol{\mathcal{B}}(t)$ from (4). For this sake, consider Fig. 2.

Note that each matrix $\mathbf{B}_q$ in a certain SC q in Fig. 2 is represented by a rectangle. Also, each matrix $\mathbf{B}_q$ is determined by a set of column vectors. These column vectors, $\mathbf{s}(\phi_r)$ with $r \in \{1, 2, \cdots, QN\}$, depend on the angle, ϕ_r, which is the angle of departure (AoD) to which the symbol $\mathbf{s}(\phi_r)$ is desired to be transmitted. Thus, we design the symbol $\mathbf{s}(\phi_r)$ as in (6)

$$\mathbf{s}(\phi_r) = \sqrt{\frac{P_s}{M}} \Big[e^{j\frac{2\pi}{\lambda_q} d\left(-\frac{M-1}{2}\right)\sin(\phi_r)}, \\ e^{j\frac{2\pi}{\lambda_q} d\left(1-\frac{M-1}{2}\right)\sin(\phi_r)}, \cdots, e^{j\frac{2\pi}{\lambda_q} d\left(\frac{M-1}{2}\right)\sin(\phi_r)} \Big]^H, \quad (6)$$

where P_s is the power of the signal, the angle ϕ_r is modeled as $\phi_r = (k-1)\pi/(QN-1)$, covering the angular space $[-\pi/2, \pi/2]$ radians where the targets are supposed to be located. However, the following formula $\phi_{q,n} = [(q-1)N + n - 1] \times \pi/(QN-1)$ indicates the angle of the symbol for the qth SC and time-slot n. Thus, the matrix $\boldsymbol{\mathcal{B}}(t) \in \mathcal{C}^{M \times N}$ is designed as

$$\boldsymbol{\mathcal{B}}(t) = \frac{1}{\sqrt{Q}} \sum_{q=1}^{Q} \left[\mathbf{s}(\phi_{q,1}), \mathbf{s}(\phi_{q,2}), \cdots, \mathbf{s}(\phi_{q,N})\right] e^{j2\pi f_q t}. \quad (7)$$

Fig. 3 illustrates the angular division as a function of SCs and time-slots. So, the M OFDM symbols transmitted by M antenna elements in a time-slot n simultaneously cover several angular positions. For example, in Fig. 3, observe that the orange beams are formed in the same time-slot $n = 1$ by different SCs, in time-slot $n = 2$ the gray beams are formed, and so on. That is, the designed symbols ensure that no other beam will occupy the angular region of another beam, and after N time-slots the region where the targets are located is covered.

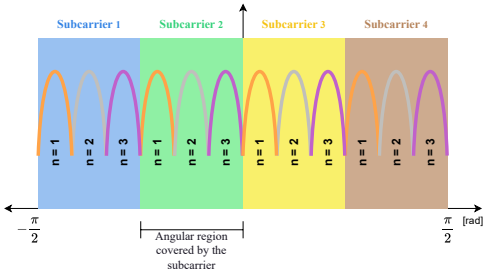

Fig. 3: Beams dependent on time-slots and SCs.

After transmitting the symbols in the N time-slots and receive the echos related to it, we apply the matched filter (MF) to the received matrices, $\mathbf{X}_q$. The design of this filter is based on the transmitted pilot signals, $\mathbf{B}_q$, that are known by the transmitter in a monostatic sensing scenario. The application of the MF is useful because we rely on the fact that the received echoes with higher power occur when the transmission beams point to the target, similar to conventional beamforming (CB) approach. (8) illustrates the application of the MF to the considered signal model.

$$\mathbf{Y}_q = \mathbf{B}_q \odot \mathbf{X}_q, \quad (8)$$

where $\mathbf{Y}_q \in \mathcal{C}^{M \times N}$ and $\odot$ is the Hadamard product. To calculate the energy of each beam generated by the transmissions of the MN OFDM symbols, we define $\mathbf{Y}$ stacking the matrices $\mathbf{Y}_q$, $\mathbf{Y} = [\mathbf{Y}_1, \mathbf{Y}_2, \cdots, \mathbf{Y}_Q] \in \mathcal{C}^{M \times QN}$. This matrix can be seen as

$$\mathbf{Y} = [\mathbf{y}(\phi_{1,1}), \mathbf{y}(\phi_{1,2}), \cdots, \mathbf{y}(\phi_{1,N}), \\ \cdots, \mathbf{y}(\phi_{Q,1}), \mathbf{y}(\phi_{Q,2}), \cdots, \mathbf{y}(\phi_{Q,N})]. \quad (9)$$

Although we use N time-slots, we have QN values to identify the angular position of the targets. Additionally, note that each column vector of the matrix $\mathbf{Y}$, $\mathbf{y}(\phi_{q,n})$, represents the received echo by the ULA when the symbols related to the angle $\phi_{q,n}$ were transmitted.

Thus, through the matrix $\mathbf{Y}$, we calculate the amplitude of the received echoes for each angle $\phi_{q,n}$ as the absolute value of the sum of the components of each column vector of $\mathbf{Y}$. Thus, the amplitude of the processed echo related to the angle $\phi_{q,n}$ is given by $|\mathbf{1}_M^T \mathbf{y}(\phi_{q,n})|$, where $|.|$ represents the module operation. By doing this process for all QN angles, we obtain QN amplitude values. Thus, we have the amplitude spectrum of the echoes as a function of the transmission angles, $\phi_{q,n}$. Therefore, the peaks of this spectrum correspond to the estimated angular positions of the targets. This relationship can be directly inferred from the found amplitude values. So, applying this method the angular resolution is $\pi/(QN-1)$ radians.

IV. Performance Evaluation

We simulated the model described in Section II and applied the solution presented in Section III. We defined the number of targets as $K = 2$. The number of antenna elements in the ULA is $M = 8$. The number of time-slots is $N = 8$. The central frequency defined is $f_c = 28\,GHz$. The spacing of the antenna elements in the ULA is given by half the wavelength of the central frequency. All targets have their positions generated in the far-field of the ULA. We define the coordinates of target 1 and 2 as $(10\,m,\ 17.3205\,m)$ and $(-10\,m,\ 56.7128\,m)$, respectively. Each target has different RCS. The main simulation parameters are shown in Table I.

TABLE I: Simulation parameters.

Parameters	Values
Carrier frequency [GHz]	28 [GHz]
Antenna elements (M)	8
Antenna element spacing ($d = \lambda/2$)	0.0054 [m]
Angular position - targets 1 and 2	30, -10 [deg]
RCS - targets 1 and 2	1, 8 [m²]
SCS (Δf)	120, 240, 480 [KHz]
Noise power dependent on SCS (α^2)	-123, -120, -117 [dBm]
AP transmit power (P_s)	1 [W]
Number of Monte Carlo repetitions	1000

The considered performance indicators are the absolute estimation error in degrees and the computational complexity in number of floating-point operations per second (FLOPS).

As the first result, in Fig. 4, we observe the empirical cumulative distribution function (ECDF) as a function of the estimation error and the quantity $Q = \{64, 128, 256\}$ of SCs with a SCS of $\Delta f = 120\,kHz$. Solid and dashed lines represent the ECDFs for target 1 and target 2, respectively. Firstly, we observe that increasing the number of SCs decreases the estimation error. For example, for target 2, the median of the estimation error for 64 SCs was approximately 0.56°, but if we increase the number of SCs to 128 and 256 SCs, the median estimation error drops to approximately 0.41° and 0.24°, respectively. This result is expected since we opted to fix the number of time-slots to $N = 8$ in consideration to limit the amount of radio resources dedicated to sensing in order not to impact the underlying communication service. However, the same level of estimation error could be obtained for the lower number of SCs if the number of time-slots allocated to sensing is adjusted accordingly in order to keep the time-frequency product constant. Alternatively, for a fixed number of SCs and time-slots, accuracy could be improved by using more antenna elements in the array. We also notice from Fig. 4 that angle estimates are more accurate for target 2 than for target 1. This is due to the fact that, although target 1 is closer to the AP than target 2, its RCS is greater. Such difference is more pronounced for a lower number of SCs.

As a second result, Fig. 5 shows the estimation error of target 1 when it is fixed a bandwidth, $B = 6\,MHz$, and it is considered three SCS $\Delta f = \{120\,kHz,\ 240\,kHz,\ 480\,kHz\}$. We note that with a fixed bandwidth and given frequency spacing, we will have a quantity Q of SCs for each configuration. For example, for $\Delta f = 120\,kHz$, there are $Q = 500$ SCs, for $\Delta f = 240\,kHz$, there are $Q = 250$ SCs, and for $\Delta f = 480\,kHz$, there are $Q = 125$ SCs. Although the ECDF of target 2 is not presented here, its ECDF is similar and leads to the same conclusions. Additionally, we again notice that increasing the SCS results in an increase in estimation error. For example, the SCS $\Delta f = \{120\,kHz,\ 240\,kHz,\ 480\,kHz\}$ produced, respectively, a median estimation error of 0.12°, 0.24°, and 0.54°.

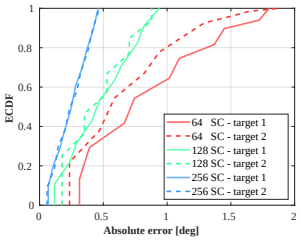

Fig. 4: ECDF of the estimation error dependent on the number of SCs.

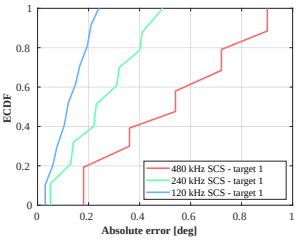

Fig. 5: ECDF of the estimation error dependent on the SCS (Target 1).

Results such as ones in Fig. 4 and 5 constitute a performance characterization that illuminates the resource allocation policy of the network operator in terms of resource sharing between communication and sensing services. The desired angle estimation error, that is the accuracy of the sensing service, is mapped against the number of radio resources, in this case SCs, allocated to it. On the other hand, the performance of the communication service as a function of the number of radio resources is well known in general from the modulation and coding scheme selected to a particular user. In that way, the operator will be able to define the optimum resource sharing policy for the co-existence of the integrated sensing and communication.

As a third result, Table II presents the computational complexity of the proposed algorithm and the MUSIC algorithm in FLOPS. The computational complexity of the algorithms depends on the size of the matrices $\mathbf{X}_q$ of received signals [16, 17].

TABLE II: Computational complexity.

Algorithm	Computational complexity
Proposed method	$\mathcal{O}(MQN)$
MUSIC	$\mathcal{O}(M^2QN + M^3)$

Notice that the computational complexities shown in Table II represents the main operations on the received echoes used to obtain the angle spectra of the proposed method and MUSIC. So the computational complexity of the generation of the spectra itself is not included in the calculations. The chosen angular resolution for MUSIC is equal or better than 2.2×10^{-3} radians.

Fig. 6 shows the mean absolute error of the algorithms as a function of the number of SCs for target 1, considering $M = 8$,

$N = 8$, and $\Delta f = 120\,kHz$. We observe that MUSIC is quite efficient because it applies ED to the covariance matrix of the received signals to find a projection matrix of the noise vector space. Notice, however, when we extrapolate the number of SCs, the proposed method presents a decreasing mean error that approaches MUSIC's. As stated above for the proposed method, even if the number of SCs is limited, improved accuracy could be obtained by either increasing the number of time-slots or the number of antenna elements.

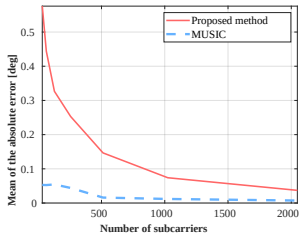

Fig. 6: Estimation error versus number of subcarriers.

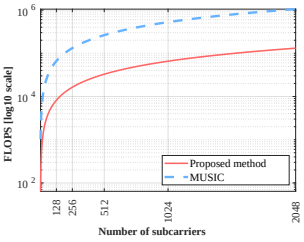

Fig. 7: Comparative computational complexity.

Finally, we present Fig. 7 which illustrates the computational complexity in FLOPS of the two algorithms as a function of the number of SCs when $M = 8$, $N = 8$. We observe that the computational complexity of MUSIC is about one order of magnitude higher than that of the proposed algorithm because the latter depends on the number of multiplications performed when the Hadamard product is carried out, while MUSIC has higher complexity as it requires computing the covariance matrix and performing ED [5].

V. Conclusion

We proposed a codebook for angular estimation of targets in a radar monostatic scenario suitable for ISAC with a MIMO-OFDM configuration. The proposed codebook explores both frequency and time dimensions to cover the angular space. Computational simulations demonstrated the impacts of the number of considered SCs and the frequency spacing of the SCs, as well as comparing the performance and complexity of the proposed algorithm to classical MUSIC.

The angle estimation error observed on the proposed method, typically less than one degree, while higher than MUSIC's, is sufficient for some applications, particularly position estimation. [18].

Moreover, the lower complexity of the proposed method in comparison to MUSIC's is a potentially much more desired property than very high accuracy, since ISAC is poised to be implemented in communications equipment already burdened by computations due to signal processing for communications.

Furthermore, the proposed method can also be a computationally light approach to initialize a multi-static ISAC architecture by helping the transmitting AP to beamform in the direction of the targets, maximizing the receiving APs ability to localize and track them.

References

[1] Cheng-Xiang Wang et al. "On the Road to 6G: Visions, Requirements, Key Technologies, and Testbeds". In: *IEEE Commun. Surveys Tuts.* (2023), pp. 905–974. DOI: 10.1109/COMST.2023.3249835.

[2] Walid Saad et al. "A Vision of 6G Wireless Systems: Applications, Trends, Technologies, and Open Research Problems". In: *IEEE Network* (2020), pp. 134–142. DOI: 10.1109/MNET.001.1900287.

[3] J. Andrew Zhang et al. "Enabling Joint Communication and Radar Sensing in Mobile Networks—A Survey". In: *IEEE Commun. Surveys Tuts.* (2022), pp. 306–345. DOI: 10.1109/COMST.2021.3122519.

[4] J. Andrew Zhang et al. "An Overview of Signal Processing Techniques for Joint Communication and Radar Sensing". In: *IEEE J. Sel. Top. Signal Process.* (2021), pp. 1295–1315. DOI: 10.1109/JSTSP.2021.3113120.

[5] R. Schmidt. "Multiple emitter location and signal parameter estimation". In: *IEEE Trans. Antennas Propag.* (1986), pp. 276–280. DOI: 10.1109/TAP.1986.1143830.

[6] Shiqi Chen et al. "Simultaneous Beam Sweeping for Multi-Beam Integrated Sensing and Communication". In: *Proc. of IEEE ICC*. 2022, pp. 4438–4443. DOI: 10.1109/ICC45855.2022.9838563.

[7] J. Andrew Zhang et al. "Multibeam for Joint Communication and Radar Sensing Using Steerable Analog Antenna Arrays". In: *IEEE Trans. Veh. Technol.* (2019), pp. 671–685. DOI: 10.1109/TVT.2018.2883796.

[8] Zhenyu Xiao et al. "Fundamentals of Array Beamforming". In: *Array Beamforming Enabled Wireless Communications*. Mar. 2023, pp. 1–50. DOI: 10.1201/9781003366362-1.

[9] Fan Liu et al. "Joint Radar and Communication Design: Applications, State-of-the-Art, and the Road Ahead". In: *IEEE Trans. Commun.* (2020), pp. 3834–3862. DOI: 10.1109/TCOMM.2020.2973976.

[10] Mark A. Richards. "Propagation Effects and Mechanisms". In: *Principles of Modern Radar: Basic principles*. Jan. 2010, pp. 3–923.

[11] X.H. Wu et al. "MIMO-OFDM radar for direction estimation". In: *IET Radar, Sonar & amp; Navigation* (2010), p. 28. DOI: 10.1049/iet-rsn.2008.0152.

[12] Alexis Bazin et al. "Doppler Effect Reduction in an OFDM System Thanks to Massive MIMO". In: *IEEE Access* (2018), pp. 38498–38511. DOI: 10.1109/ACCESS.2018.2854001.

[13] 3rd Generation Partnership Project (3GPP). *TS 38.211: NR; Physical channels and modulation (Release 17)*. Tech. rep. Version 17.4.0. 3GPP, 2022.

[14] Yunxin Li et al. "Frame Structure and Protocol Design for Sensing-Assisted NR-V2X Communications". In: *IEEE Transactions on Mobile Computing* (2024), pp. 1–17. DOI: 10.1109/TMC.2024.3389697.

[15] Zhongshan Zhang et al. "Full-Duplex Wireless Communications: Challenges, Solutions, and Future Research Directions". In: *Proceedings of the IEEE* (2016), pp. 1369–1409. DOI: 10.1109/JPROC.2015.2497203.

[16] Xiaocan Li et al. *Tutorial: Complexity analysis of Singular Value Decomposition and its variants*. 2019.

[17] R. Hunger. *Floating Point Operations in Matrix-vector Calculus*. Munich University of Technology, Inst. for Circuit Theory and Signal Processing, 2005.

[18] 3rd Generation Partnership Project (3GPP). *Technical Specification Group TSG SA; Feasibility Study on Integrated Sensing and Communication (Release 19)*. 3GPP Technical Report. Version v19.0.0. 3GPP, Mar. 2023.